Journal of Thermal Analysis, Vol. 52 (1998) 425-438

CONSIDERATIONS ON THE THERMAL BEHAVIOUR AND OXIDATION RESISTANCE OF CAST IRON

M. Muscalu and D. Fatu

Department of Physical Chemistry, Faculty of Chemistry, University of Bucharest
Bul. Carol No. 13. Bucharest, Romania

Dedicated to Professor Eugen Segal for his 65th birthday

Abstract

Thermal analysis was used to characterize the thermal behaviour and oxidation resistance of some nodular cast irons. Samples of nodular cast iron in various stages of elaboration, with different chemical compositions, were studied. The samples were heated in air, in the temperature range 291–1273 K, and the thermal (TG, DTG and DTA) curves were recorded.

A group of samples with low silicon content exhibit similar behaviour: a continuous increase in mass and an exothermic effect up to 1123 K. The thermal effects correspond to iron oxide (Fe_3O_4, FeO, Fe_2O_3) formation. At high temperatures (T>1123 K), there is a decrease in mass and an endothermic effect. A decrease in the superficial carbon content by combustion ('decarburization' effect) occurs in the range of high temperatures. The two effects of oxidation and decarburization depend on the structural changes which occur in cast iron at high temperatures.

The decarburization process was modelled and the kinetic parameters were determined (reaction order n=0.76; activation energy E=141 kJ mol^{-1}; pre-exponential factor A= 2·10^2 s^{-1}).

The oxidation process was studied by non-isothermal methods with regard to two mechanisms: two-dimensional transport for low temperatures, and three-dimensional transport through a sphere for high temperatures. The activation energies were calculated: 68 kJ mol^{-1} for low temperatures and 122 kJ mol^{-1} for high temperatures.

Keywords: kinetics, nodular cast iron, TG-DTG-DTA

Introduction

Good mechanical properties, good casting properties and special oxidation resistance are the main features of nodular cast iron. Nodular cast iron generally has a good oxidation resistance up to 923 K; a higher resistance than that for grey cast iron or low alloy steel [1].

The oxidation resistance of nodular cast iron is related to the nodular shape of graphite and it depends on the chemical composition and microstructural features of the material.

1418–2874/98/ $ 5.00
Akadémiai Kiadó, Budapest

Table 1 Chemical composition of the cast iron samples (% mass)

Sample	C%	Si%	Mn%	P%	S%	Cu%	Mg%	C.E.%
F_1	3.78	0.74	1.20	0.020	0.026	0.026	0.027	4.03
F_2	3.79	0.88	1.25	0.021	0.024	0.370	0.028	4.09
F_3	3.94	1.45	1.00	0.021	0.034	0.046	0.026	4.43
F_4	3.50	2.80	0.50	0.021	0.032	0.450	0.050	4.44

C.E.=carbon equivalent=C%+1/3(Si+P)%

The nodular shape of graphite is a result of special treatment of the molten metal before casting. The treatment consists in two processes: the addition of a (MgFeSi) alloy ('modification') and the addition of an (FeSi) alloy ('postmodification' or 'inoculation') [2, 3].

Nodular cast iron samples F_1–F_3 after the modification process, without ferrosilicon addition, and sample F_4 after modification and inoculation (final stage of elaboration), have been investigated.

The samples of nodular cast iron were powders resulting from the breaking of plates, with 'white' structure, the particles measuring no more than 0.5 mm. These plates exhibit a fast solidification when cooling and therefore the structure is 'white' (iron carbide Fe_3C = cementite is the main structural component).

The chemical compositions of the samples are shown in the Table 1.

Primary solidification of hypoeutectic samples (F_1, F_2) leads to austenitic dendrites and ledeburitic eutectic (with carbon content 4.3%) in accordance with the Fe–Fe_3C diagram. When cooling continues austenite turns into pearlite and secondary cementite. The microstructure of these samples consists of acicular crystals of cementite and some pearlite. The microstructure of hypereutectic samples (F_3, F_4) consists of primary cementite and ledeburite [4].

Experimental

The powdered samples of cast iron were heated from room temperature to 1273 K at a linear heating rate. The experimental conditions and total mass variations, are given in Table 2.

Table 2 Experimental conditions for thermal analysis of nuclear cast iron samples

Sample	T_{range}/ K	Heating time/ min	Heating rate/ K min^{-1}	Total mass variation/ mg
F_1	291–1273	100	283	15.3
F_2	291–1273	200	278	37.1
F_3	291–1273	200	278	36.3
F_4	290–1273	200	278	30.0

The equipment used was a derivatograph (MOM, Paulik Paulik C, Budapest) with null thermobalance, with a static air atmosphere in the sample chamber; the reference material was Al_2O_3.

Figures 1–4 give the thermal curves for cast iron samples F_1...F_4.

The powders and the plates were also kept in a furnace, at the temperatures, corresponding to the thermal effects in the thermal curves. The samples were then examined by optical microscopy.

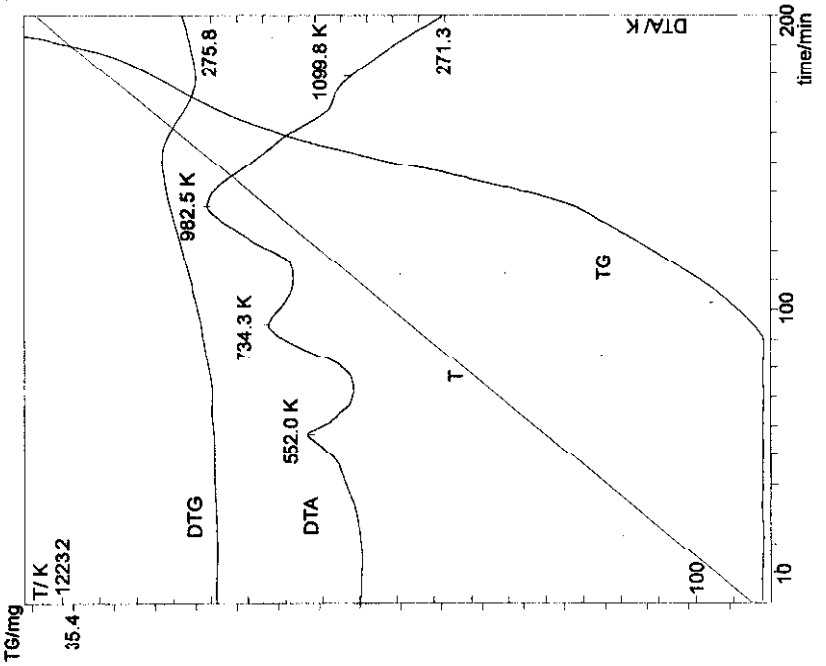

Fig. 1 Thermal curve for F_1 sample

Fig. 2 Thermal curve for F_2 sample

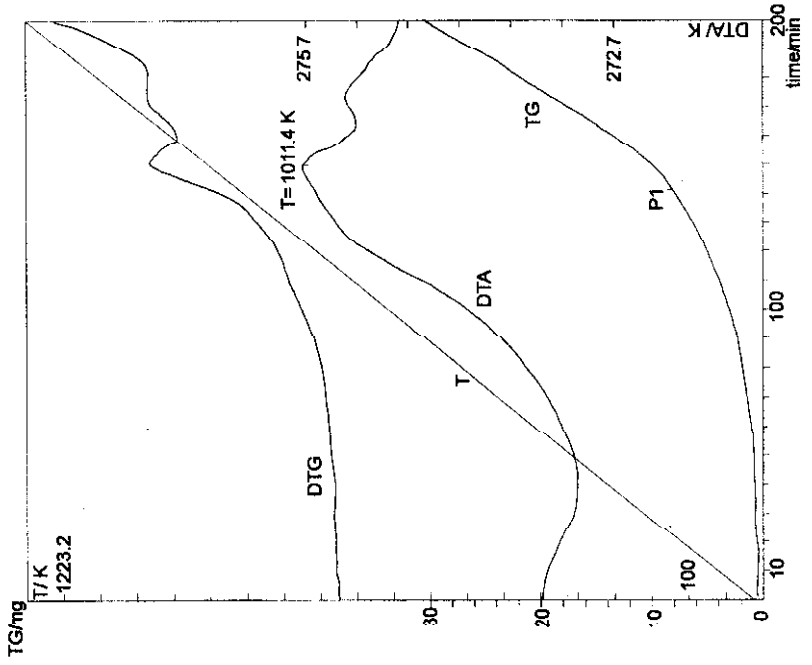

Fig. 4 Thermal curve for F_4 sample

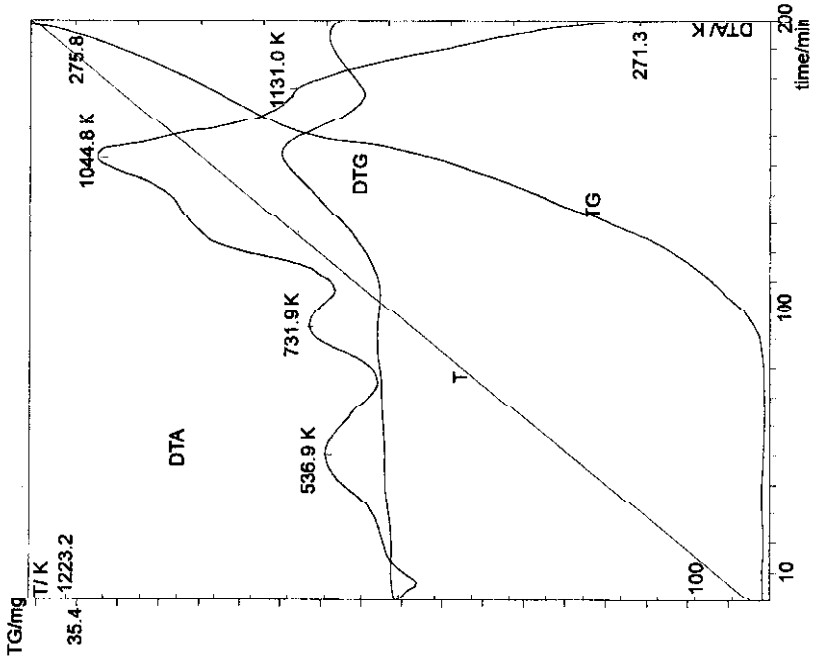

Fig. 3 Thermal curve for F_3 sample

Results and discussion

Samples F_1–F_3 exhibit similar behaviour, whereas sample F_4 behaves differently.

Table 3 gives data from the thermal curves: temperatures of interest, the mass change Δm and the temperature variation ΔT.

A. The result of linear heating of samples F_1–F_3 is a continuous increase in significant mass up to 1123 K, followed by a decrease in mass. The DTA curves reveal an exothermic effect up to about 1123 K.

– At low temperature (533–543 K), there is a composition change without mass change, due to the oxidation of non-metallic components (S, P).

– At about 733 K, iron oxidation begins; the iron is oxygen-saturated and Fe_2O_3, according to the Fe–O diagram; correspondingly, an exothermic effect and a mass increase are recorded.

– At T>843 K, FeO is formed in small quantities.

– The next important temperature is 1023 K, where a large amount of Fe_2O_3 is observed.

– The maximum oxidation peak in the DTA curve is recorded at T>1093 K, for samples F_2 and F_3.

The differences between samples F_1–F_3 could be correlated with the silicon content. Samples F_2 and F_3, with higher silicon content, give the same thermal effects at higher temperatures; the end of the exothermic effects is also located at higher temperatures: 1100 K for sample F_2, 1131 K for sample F_3 and 1031 K for sample F_1.

On the other hand, the microscopic observations are:

– At low temperature, the samples do not show structural changes.

– At 733 K, a thin oxide layer can be observed on the powder surface; no structural changes in the plates occur.

– For the temperature range 873–973 K, the amount of oxide increases and the particles of cementite become smaller.

– An important structural change in sample F_1 occurs at 1214 K (the cementite transformation) [5]:

$$Fe_3C \rightarrow C(\text{graphite}) + Fe\gamma(\text{austenite}) \quad (1)$$

The austenite phase is stable only at high temperatures; on cooling, it turns into pearlite and ferrite. The final microstructure of sample F_1 consists of graphite (nodular shape), pearlite and ferrite.

– The F_2 plate, kept at 1103 K, shows some transformation described by reaction (1). The microstructure consists of graphite and a few sections with pearlite and ferrite.

Table 3 Thermal effects and mass change

Sample	T/K	541.4	751.7	860.3	1031.0	1215.0	
F_1	ΔT/K	273.3	277.1	285.2	274.7	270.7	
	$\Delta m \cdot 10^3$/g	0	2.0	7.3	15.3	11.3	
Sample	T/K	552.0	734.3	893.2	982.5	1099.8	
F_2	ΔT/K	274.1	274.6	274.8	275.7	273.9	
	$\Delta m \cdot 10^3$/g	0	1.8	7.6	15.4	26.4	
Sample	T/K	536.9	731.9	944.0	1044.8	1131.0	
F_3	ΔT/K	273.6	273.8	274.6	275.0	275.6	
	$\Delta m \cdot 10^3$/g	0	1.1	5.8	10.3	17.0	
Sample	T/K	599.6	964.7	1011.4	1067.7	1095.5	1192.9
F_4	ΔT/K	273.2	275.5	275.7	275.2	271.1	274.4
	$\Delta m \cdot 10^3$/g	0	6.0	9.3	13.7	15.8	24.0

At the same time, we must take into account the decrease in superficial carbon content produced by carbon combustion (for $T>1143$ K). This 'decarburization' effect leads to a mass loss which can exceed the increase in mass due to iron oxidation.

The rate of the decarburization process of nodular cast iron depends on two factors: dissolution of graphite into the matrix, and carbon diffusion through the matrix to the surface [1].

The combination of the two effects, oxidation – decarburization, is more interesting in the case of sample F_1. We determined the kinetic parameters for the last section of the TG curve (Fig. 1).

Table 4 The temperature and the weight change for F_1 sample (from the last section of TG curve)

T/K	$\Delta m \cdot 10^3$/g
1022.3	15.25
1031.6	15.23
1040.4	15.16
1050.5	15.03
1059.2	14.87
1069.2	14.70
1079.8	14.51
1089.3	14.30
1098.4	14.07
1108.0	13.86
1117.4	13.62
1127.4	13.37
1136.8	13.12
1146.3	12.82
1156.1	12.51
1166.3	12.20
1175.5	11.89
1185.0	11.60
1194.3	11.37
1204.3	11.20
1212.6	11.06
1223.7	10.99
1232.8	10.95

Table 5 The temperature, the mass change and the degree of conversion for F_4 sample-part I

No.	$(1/T)\cdot10^4(K^{-1})$	$\Delta m\cdot10^4$/g	$-\log[F(\alpha)/T^2]$	α
1	15.2	0.13		0.0004
2	14.9	0.53		0.002
3	14.7	1.00		0.003
4	14.5	1.64		0.006
5	14.3	2.35		0.008
6	14.1	3.19		0.011
7	13.9	4.02		0.013
8	13.7	4.98		0.017
9	13.6	5.97		0.020
10	13.4	7.09		0.024
11	13.2	8.38		0.028
12	13.0	9.78		0.033
13	12.9	11.05	8.272	0.037
14	12.7	11.94	8.270	0.040
15	12.5	14.71	8.246	0.049
16	12.4	17.03	8.200	0.057
17	12.2	18.96	8.160	0.063
18	12.1	21.56	8.146	0.072
19	11.9	24.28	8.097	0.081
20	11.8	27.33	8.034	0.091
21	11.7	30.24	7.987	0.101
22	11.5	33.24	7.933	0.111
23	11.4	36.54	7.850	0.122
24	11.3	39.96	7.830	0.133
25	11.1	43.44	7.788	0.145
26	11.0	46.80	7.740	0.156
27	10.9	50.13	7.695	0.167
28	10.8	53.48	7.652	0.178
29	10.7	56.95	7.613	0.190
30	10.5	60.60	7.578	0.202
31	10.4	64.41	7.535	0.215
32	10.3	68.41	7.495	0.228
33	10.2	72.88	7.449	0.243

Table 5 Continued

No.	$(1/T)\cdot 10^4(K^{-1})$	$\Delta m\cdot 10^4$/g	$-\log[F(\alpha)/T^2]$	α
34	10.1	78.01	7.399	0.260
35	10.0	84.16	7.801	0.281
36	9.9	91.15	7.730	0.304
37	9.8	98.96	7.630	0.329
38	9.7	107.27	7.580	0.358
39	9.6	115.32	7.510	0.384
40	9.5	123.41	7.440	0.411
41	9.4	131.00	7.400	0.437
42	9.3	138.39	7.350	0.461
43	9.25	146.03	7.280	0.487
44	9.2	153.98	7.240	0.513
45	9.1	162.30	7.200	0.541
46	9.0	170.88	7.140	0.570
47	8.9	179.58	7.085	0.598
48	8.8	188.33	7.029	0.628
49	8.75	196.89	6.977	0.656
50	8.7	205.32	6.930	0.684
51	8.6	213.56	6.890	0.712
52	8.55	221.81	6.850	0.739
53	8.5	230.12	6.800	0.767
54	8.4	238.77	6.750	0.796
55	8.3	248.11	6.680	0.827
56	8.25	258.28	6.630	0.861
57	8.2	269.42	6.545	0.898
58	8.1	281.83	6.450	0.939
59	8.0	295.41	6.263	0.985

Table 4 gives the data from the TG and T curves for sample F_1. A program (written in BASIC language) allowed determination of the kinetic parameters. The model of the contracting sphere based on Eq. (2) was used [6]:

$$1-(1-\alpha)^{1/3}=kt \tag{2}$$

$$\frac{d\alpha}{dt}=k(1-\alpha)^{2/3} \tag{3}$$

where α is the degree of conversion, t is time and k is the rate constant.

The following values of the kinetic parameters were obtained:

– activation energy: 141 kJ mol^{-1};

– reaction order: 0.76;

– pre-exponential factor: 2 10^2 s^{-1}.

B. Sample F_4 with a typical chemical composition of nodular cast iron, has a particular oxidation resistance.

The DTA curve shows an important effect at $T = 1011$ K; the oxidation begins in practice at $T = 798$ K and proceeds slowly up to $T = 989$ K. The point Pl corresponding to $T = 989$ K delimits two sections in the TG curve, which are characterized by different oxidation kinetics.

Nodular cast iron oxidation was studied by using the non-isothermal kinetics of heterogeneous reactions which involve solid phases. They are described by special equations [7, 8].

The integral kinetic equation for non-isothermal conditions, using the Coats-Redfern approximation, is

$$\log\frac{F(\alpha)}{T^2} = \log\frac{AR}{aE}\left(1 - \frac{2RT}{E}\right) - \frac{E}{2.303R}\frac{1}{T} \tag{4}$$

where $F(\alpha)$ is the integral of the conversion, given by

$$F(\alpha) = \int_0^{\alpha} \frac{d\alpha}{f(\alpha)} \tag{5}$$

where α is the degree of conversion, and $f(\alpha)$ is a function which shows the dependence of the reaction rate on the conversion degree;

A is the pre-exponential factor; E is the activation energy;

$a = dT/dt$ is the constant heating rate;

T is absolute temperature; and R is the perfect gas constant.

The plot $[\log F(\alpha)/T^2, 1/T]$ should be linear, which gives the activation parameters (A and E).

The model of the reaction controlled by diffusion was used in two variants:

a) Two-dimentional transport;

b) Three-dimensional transport through a sphere.

The integrals of the conversion are:

$$\text{a) } F(\alpha) = \alpha + (1 - \alpha)\ln(1 - \alpha) \text{ for two-dimensional transport} \tag{6}$$

$$\text{b) } F(\alpha) = 3\left\{\frac{1}{2}\left[1 + (1 - \alpha)^{2/3}\right] - (1 - \alpha)^{1/3}\right\} \tag{7}$$

for three-dimensional transport.

The corresponding equations are

$$\text{a) } \log\frac{1}{T^2}[\alpha + (1-\alpha)\ln(1-\alpha)] = \log\frac{AR}{aE}\left(1-\frac{2RT}{E}\right) - \frac{E}{2.303R}\frac{1}{T} \quad (8)$$

$$\text{b) } \log\frac{1}{T^2}\left\{\frac{1}{2}\left[1+(1-\alpha)^{2/3}\right]-(1-\alpha)^{1/3}\right\} = \log\frac{AR}{aE}\left(1-\frac{2RT}{E}\right) - \frac{E}{2.303R}\frac{1}{T} \quad (9)$$

Relationship (9) corresponds to the Jander equation.

Table 5 lists the data from the thermal curves: the mass change, the degree of conversion and the data for computing the kinetic parameters.

First we tried to describe the oxidation kinetics by using the Jander equation for the two temperature ranges shown in Figs 5 and 6. The Jander equation can be seen to describe the oxidation kinetics better for the second temperature range (T=989–1273 K). This equation is not appropriate for the first temperature range, where weak oxidation occurs.

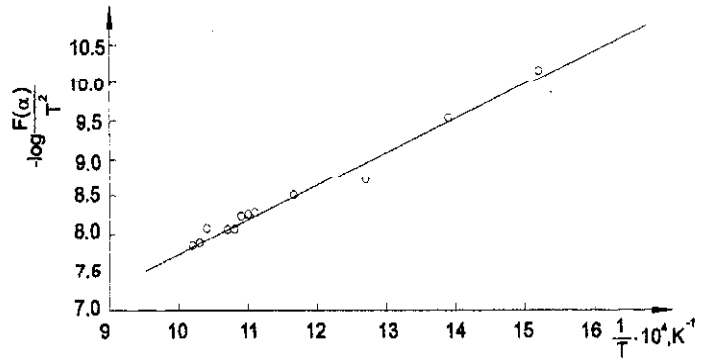

Fig. 5 The dependence $\left[\log\frac{F(\alpha)}{T^2}, \frac{1}{T}\right]$ for low temperatures (Jander equation)

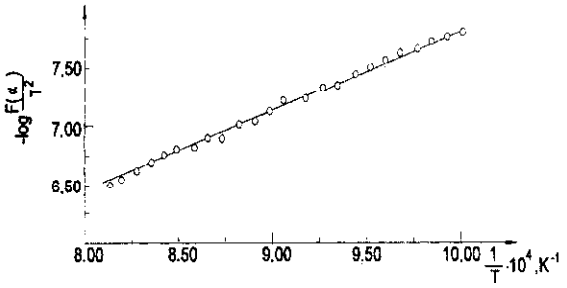

Fig. 6 The dependence $\left[\log\frac{F(\alpha)}{T^2}, \frac{1}{T}\right]$ for high temperatures (Jander equation)

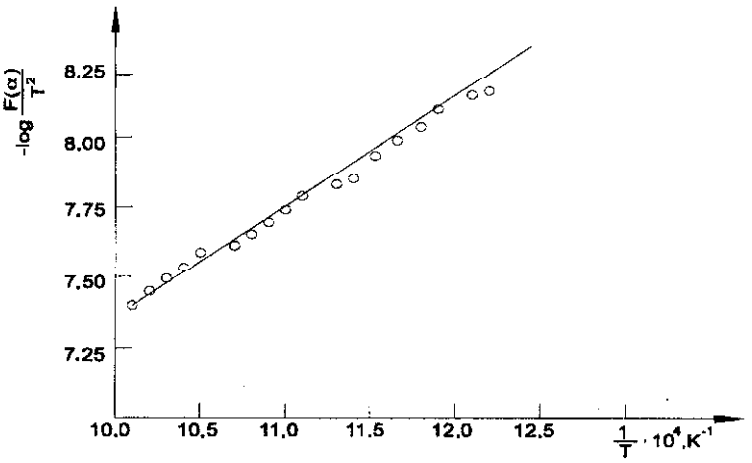

Fig. 7 The dependence $\left[\log\frac{F(\alpha)}{T^2}, \frac{1}{T}\right]$ for low temperatures (two-dimensional transport)

The model of two-dimensional transport better fits the first temperature range (T<989 K) (Fig. 7).

The kinetic parameters calculated for the two mechanisms are given in Table 6.

Table 6 Kinetic parameters for F_4 sample

Temperature range/K	E/kJ mol^{-1}	A/s^{-1}
659–989	68	$3.8\cdot10^3$
989–1273	122	$2.9\cdot10^3$

Conclusions

1. Thermal analysis and microscopic observations were used to characterize some less studied features of nodular cast iron: thermal behaviour and oxidation resistance.

The study was based on analysis of the heating curves, as they contain more information than the cooling curves frequently used for metallurgical purposes.

2. In general, all the samples (which are nodular cast iron melts) have a good oxidation resistance up to 873–943 K. This property depends on the silicon content. Samples F_1–F_3, modified with magnesium alloy and without ferrosilicon addition, show similar features in the thermal curves: some thermal effects corresponding to the formation of iron oxides (Fe_3O_4, FeO, Fe_2O_3). Sample F_1 (with lower silicon content) exhibits a lower oxidation resistance.

Sample F_4 with a specific nodular cast iron composition, displays good oxidation resistance up to 989 K.

3. The decarburization process must be taken into account at high temperature (T>1143 K) and is correlated with the first phase transformation (reaction 1).

4. The kinetics of decarburization and oxidation were modelled and the kinetic parameters of these processes were calculated.

The model of the contracting sphere was used for the decarburization process; two mechanisms (two-dimensional transport and three-dimensional transport through a sphere) were used to describe the oxidation kinetics of nodular cast iron.

References

1 L. Sofroni, D. M. Stefanescu and C. Vincenz, 'Nodular Cast Iron', Technical Publishing House, Bucharest 1978.
2 L. Sofroni and D. M. Stefanescu, 'Modified Cast Iron', Technical Publishing House, Bucharest, 1971.
3 D. Taloi, F. Oprea, I. Constantin and R. Roman, 'Metallurgic Process Theory', Didactical and Pedagogical Publishing House, Bucharest 1978.
4 S. Gadea and M. Petrescu, 'Physical Metallurgy and Study of Metals', Didactical and Pedagogical Publishing House, Bucharest 1981.
5 N. Geru, 'Physical Metallugry', Didactical and Pedagogical Publishing House, Bucharest, 1981.
6 I. G. Murgulescu, E. Segal and T. Oncescu, 'Chemical Kinetics and Catalysis', Academy Publishing House, Bucharest 1980.
7 E. Segal and D. Fatu, 'Introduction to Nonisothermal Kinetics', Academy Publishing House, Bucharest 1983.
8 E. L. Charlsley and S. B. Warington, 'Thermal Analysis' (Techniques and Applications), Royal Society of Chemistry, Cambridge 1992.